Wiley
International Journal of Energy Research
Volume 2024, Article ID 2406135, 16 pages
https://doi.org/10.1155/2024/2406135

WILEY

Research Article

Engineered Biomass Waste-Derived Activated Biochar Catalyst for Biodiesel Production from *Jatropha curcas* Oil

Supongsenla Ao,[1] **Sudeshna Ghorui**,[1] **Hui Li**,[2] **Gurunathan Baskar**,[3] and **Samuel Lalthazuala Rokhum**[1]

[1]*Department of Chemistry, National Institute of Technology, Silchar, Assam 788010, India*
[2]*School of Thermal Engineering, Shandong Jianzhu University, Jinan 250101, China*
[3]*Department of Biotechnology, St. Joseph's College of Engineering, Chennai 600119, India*

Correspondence should be addressed to Samuel Lalthazuala Rokhum; rokhum@che.nits.ac.in

Received 27 May 2024; Revised 4 July 2024; Accepted 6 August 2024

Academic Editor: Prakash Bhuyar

Copyright © 2024 Supongsenla Ao et al. This is an open access article distributed under the Creative Commons Attribution License, which permits unrestricted use, distribution, and reproduction in any medium, provided the original work is properly cited.

$ZnCl_2$ impregnation of the cellulosic precursor is an effective way to generate carbon catalysts with a mesoporous structure and high specific surface area. Herein, we attempt to explore the synthesis of *Citrus Limonum Pericarpium* (lemon peel), an activated biochar catalyst produced via pyrolysis and consequent sulfonation. The obtained biochar catalyst exhibited notable characteristics, including a high surface area of 863.0 $m^2\,g^{-1}$ and a substantial sulfur content of 4.02 wt.% (1.25 mmol g^{-1}) by EDX. Following, analytical techniques, such as scanning electron microscopy, BET, X-ray diffraction, Fourier-transform infrared, and TGA, were conducted for a comprehensive analysis of the catalyst. Subsequently, we applied the catalyst to optimize the transesterification process of *Jatropha curcas* oil (JCO), yielding an impressive 95.2% ± 0.4% yield. The optimization parameters were established with a reaction duration of 60 min, a temperature of 100°C, 8 wt.% catalyst, and JCO: MeOH ratio of 1 : 20. Catalyst reusability was probed over seven subsequent cycles with the final yield observed of over 88.4% ± 0.6%, while the decrease in yield was explained by EDX analysis. In summary, our investigation successfully navigated the synthesis and practical application of a sulfonated porous biochar catalyst for JCO transesterification, achieving noteworthy yields while addressing environmental concerns.

1. Introduction

Fossil fuels have historically played a pivotal role in meeting the world's energy demand; however, the utilization of petrochemical resources, coal and natural gas derived from fossil fuels, has been associated with detrimental effects such as substantial greenhouse gas emissions, contributing significantly to climate change and global warming [1]. As a result, researchers now focus on the complementary of fossil fuels like biofuels. Among various biofuels, biodiesel stands out as particularly noteworthy due to its ability to generate lower levels of CO_2 and H_2O compared to conventional diesel, and it also has nontoxicity, renewability, biodegradability, and sustainability properties [2].

Long-chain fatty acid methyl ester (FAMEs) is the primary ingredient in biodiesel, which is obtained through the transesterification process [3]. The process involves the reaction of triglycerides present in vegetable oils or animal fats, with methanol facilitated by a catalyst (Figure 1). Different types of oils are used as feedstocks to produce biodiesel, categorized into edible oils like soybean oil [3], sunflower oil [4], and inedible oils such as waste cooking oil [5] and *Jatropha curcas* oil (JCO) [6]. Lately, JCO with high free fatty acid (FFA) has gained popularity for biodiesel production due to its simplification of transesterification and cost reduction.

Over time, a range of catalysts, both homogeneous and heterogeneous, have been employed for the transesterification reaction. However, limitations associated with homogeneous catalysts, including high costs, reactor corrosion, and challenges in catalyst recovery, have prompted a shift towards heterogeneous catalysts [7]. Heterogeneous catalysts have gained attraction due to their superior catalytic efficiency, reusability, selectivity, and ease of separation, thereby advancing industrial applications [8, 9]. Recently, various biomass-derived heterogeneous catalysts, such as GZF-SO_3H catalyst

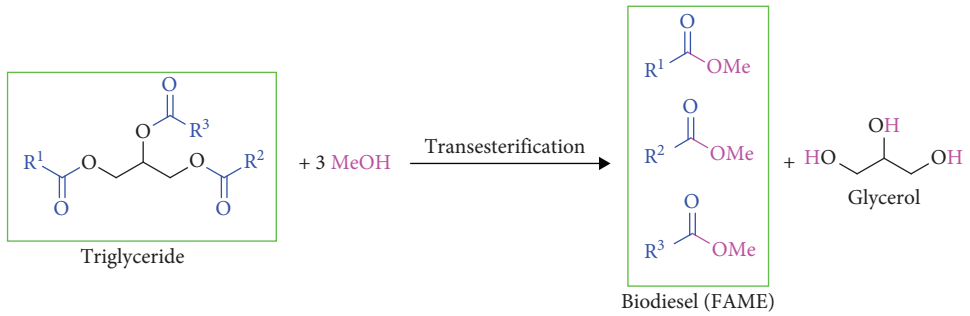


Figure 1: Synthesis of biodiesel through a transesterification reaction.

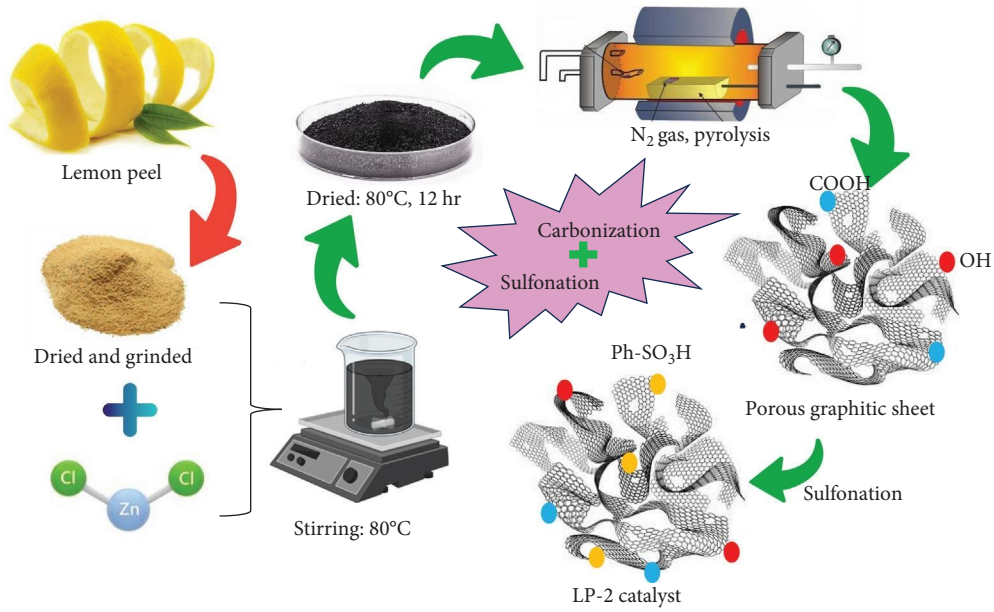


Figure 2: Schematic representation of biochar catalyst via carbonation and sulfonation.

[6] with a surface area as high as 1,196.13 $m^2 g^{-1}$ and FZBS800@SO_3H catalyst [10] with a surface area of 647.46 $m^2 g^{-1}$ was reported for the transesterification of JCO. Meanwhile, Chen et al. [11], Maleki et al. [12], Choksi et al. [13], and Ao et al. [14] also synthesized various biomass-derived carbonaceous catalysts for biodiesel production, offering several advantages such as high reusability, low-cost feedstock, increased active sites for reaction and high catalytic efficiency due to large surface area. Despite these advantages, there have been serious concerns about high energy consumption during the production due to longer reaction times and a decrease in yield upon reuse, restricting industrial applicability [14]. Hence, building upon this background, our study aims to contribute to the scientific discourse by introducing a novel catalyst derived from waste biomass (lemon peel) to overcome the existing limitations.

This research aims to find a more economical approach through a combination of chemical and physical methods, including carbonization in an N_2 atmosphere in the presence of $ZnCl_2$ to obtain a porous activated biochar. This porous architecture is highly desirable as it enhances surface area, thereby improving catalytic efficiency by increasing the presence of active sites and making it advantageous for industrial applications (Figure 2). The utilization of biomass not only renders this process environmentally friendly but also underscores the sustainable nature of activated porous carbon materials as versatile components in numerous industrial and scientific endeavors.

2. Experimental

2.1. Materials Used. Lemon peel and JCO were obtained from the local market in Silchar, Assam, India. For the experiment, 99.9% pure $ZnCl_2$ was supplied from Sisco Research Laboratories. Sulfanilic acid (99% purity), H_3PO_2 (99%), MeOH (99.9%), and ethanol (99%) were acquired from Research Lab Fine Chemicals and used without additional purification. A Simplicity® UV Water Purification System from Research Lab Fine Chemicals was used to obtain DI water.

2.2. Catalyst Preparation. Initially, the obtained lemon peel was sliced into pieces, followed by cleaning and drying in an oven at 80°C for 12 hr. Afterward, the dried material was finely ground into powder (sieved using a 150-mesh size sieve). The powdered

lemon peel (1 g) was dissolved in three different beakers of 50 mL $ZnCl_2$ (1, 2, and 3 g) solutions in the ratios of 1 : 1, 1 : 2, and 1 : 3. The mixture in three beakers were continuously stirred until evaporation and left for drying overnight at 80°C. Subsequently, it was kept in an N_2 purged tube furnace for pyrolysis for 2 hr at 500°C with heating conducted at a rate of 10°C min^{-1} for activation. After completion of the activation process, the activated product was cooled and immersed in a 2 M HCl solution overnight, and the acid was washed off with DI water to remove all the unreacted chloride ions (perform silver nitrate test [6]).

Lastly, sulfonation of the activated carbon was carried out. The sulfonating agent, 4-BDS (benzene diazonium sulfonate), was prepared through the diazotization of sulfanilic acid. Here, in a small beaker, 2.1 g of sulfanilic acid was taken, and a mixture of water and HCl (1 : 1) was added and stirred for 30 min, maintaining a temperature range of 0–5°C, in an ice bath. After which, a solution of 1.01 g of $NaNO_2$ in 20 mL water was prepared and added dropwise to the beaker, resulting in the formation of a white precipitate. The precipitate was filtered using filter paper and washed 2–3 times with cold water and acetone. The product was kept for drying overnight, thereby forming 4-BDS. Subsequently, the 4-BDS (1 g) was dissolved into a mixture of 20 mL of DI water and 12 mL of ethanol under cold conditions. To the mixture, 0.5 g of activated carbon was added, followed by the addition of a 30%–32% aqueous solution of H_3PO_2 (10 mL), which was stirred for 30 min. Another 5 mL of the H_3PO_2 aqueous solution was added and allowed to stand for 1 hr with occasional stirring. The resulting product (Figure 2) was washed using acetone and DI and then vacuum-dried overnight and labeled as LP-1, LP-2, and LP-3 with respect to the weight of $ZnCl_2$ used.

2.3. Characterization of the Synthesized Compound. Based on the modified Boehm titration procedure, the density of —COOH, —SO_3H, and —OH groups on the surface of LP1, LP-2, and LP-3 was determined [15, 16]. The total acid density was determined using basic solutions of NaOH. Equation (1) was used to calculate the total surface acid density of the catalyst.

$$n = \frac{n_{\mathrm{HCl}}}{n_B}[B]V_B - ([\mathrm{HCl}]V_{\mathrm{HCl}} - [\mathrm{NaOH}]V_{\mathrm{NaOH}})\frac{V_B}{V_{\mathrm{aliquot}}}, \quad (1)$$

where $\frac{n_{\mathrm{HCl}}}{n_B}$ is the molar ratio of HCl to base reacted; $[B]$ and V_B are the concentration and volume of the reaction base mixed with the catalyst, respectively, V_{aliquot} is the volume of the aliquot taken from the V_B, [HCl] and V_{HCL}, are the concentration and volume of acid used in the acidification, and [NaOH] and V_{NaOH} are the concentration and volume of the NaOH used in the titration.

X-ray diffraction (XRD) was used to analyze the structure and morphology of the catalyst. A PANalytical X'Pert Pro diffractometer was used, operating at 40 kV and 100 mA and using Cu Kα radiation within the 2θ range of 20°−60°. A 3000 Hyperion FTIR spectrometer (Bruker, Germany) was used to obtain Fourier-transform infrared (FTIR) spectra, which were then used to identify functional groups in the elements within the 400–4,000 cm^{-1} range. TGA of the catalyst was performed using a TG/DTA (model no. STA 409 Netzsch Geratebau GMBH, Germany) under airflow at 1.5 bar and 2 L hr^{-1} with the degassing temperature between 50 and 900°C. Energy-dispersive X-ray spectroscopy (EDS) determined which element was present on the surface of the catalyst, and scanning electron microscopy (SEM) was used to evaluate the catalyst's size, shape, and elemental composition. A JEOL JSM-7600F instrument was used for SEM analysis, and an ETD detector and tungsten-doped lanthanum hexaboride (LaB6) X-ray source were used to create SEM images with the FEI Quanta 200F instrument. SEM imaging was carried out using secondary electrons and an acceleration voltage of 30 kV in a high vacuum. The catalyst underwent a 10 hr degassing process at 150°C on a Micromeritics ASAP 2010 surface area and porosity detector. Subsequently, the BET method was employed to examine the pore volume, pore size, and surface area of the catalyst analyzed by Brunauer–Emmett–Teller.

2.4. Transesterification of J. curcas Oil to Biodiesel. Using a microwave irradiation method, 250 μL of *J. curcas* oil, 202 μL of MeOH, and 0.018 g (8 wt.% with respect to JCO) of catalyst were typically set for the transesterification under reaction condition of 100°C reaction temperature, 60 min reaction time, 1 : 20 JCO : MeOH molar ratio and a power of 50 W in a microwave tube. The reaction mixture was separated from the catalyst through the Whatman filter paper. A rotary evaporator was used to extract the product's excess MeOH. The catalyst used for the recycling experiment was washed with MeOH and hexane (2 × 15 mL) and dried overnight in an oven.

2.5. Characterization of FAME. FAME was characterized by ^{1}H NMR techniques using a JEOL ECLZR series instrument with a 500 MHz spectrometer frequency. Tetramethyl silane served as the calibration reference standard. Additionally, gas chromatography–mass spectroscopy (GC–MS) analysis was carried out to learn more about the synthesized FAME's molecular structure. An Agilent 7890 instrument in headspace injector mode and a CPSIL 8 CB capillary column with dimensions of 30 m in length, 0.25 mm in diameter, and 0.25 m in film thickness were used to perform this analysis. To identify and measure the GC–MS components, a GC-flame ionization detector (GC-FID) was connected to the GC analysis. Throughout the course, after a minute, the oven's temperature rose at a rate of 10°C from 55 to 230°C. In addition, several ASTM procedures, including D1980-87 (1998), D445, and D2500, among others, were used to evaluate the properties of the synthesized FAME. The percentage yield of the synthesized FAME could be determined using Equation (2) [17]. On the other hand, the percentage conversion of fatty acid methyl esters from the ^{1}H NMR data was determined using Equation (3).

$$\text{FAME yield } (\%) = \frac{(\text{weight of FAME})}{(\text{weight of } \textit{Jatropha curcas} \text{ oil})} \times 100, \quad (2)$$

$$\text{Conversion } (\%) = \frac{2A_{\text{Me}}}{3A_{\text{CH}_2}} \times 100. \quad (3)$$

Here A_{Me} and A_{CH_2} represent the integration values of methoxy protons and methylene protons, respectively.

2.6. Reaction Kinetics. The kinetic study of the transesterification reaction through JCO to biodiesel with the presence of a catalyst was studied here. Surplus methanol was used in the transesterification reaction, which allows the reverse reaction to be ignored [18, 19], proceeding by pseudo-first-order kinetics. The response could be expressed as follows:

$$r = \frac{-d[\text{JCO}]}{dt} = k\,[\text{JCO}]. \quad (4)$$

Here [JCO] is the concentration of JCO, r, and k are the rates and pseudo-first-order rate constants, respectively. Methyl ester yield showed first-order kinetics at time t.

$$\ln(1 - x) = kt. \quad (5)$$

The graph was plotted between $-\ln[1-x]$ vs. t, and the slope was calculated to determine the rate constant. Hence, the activation energy required for the transesterification process was determined by considering the Arrhenius equation (Equation (6)) [20]. This equation can be written as follows:

$$\ln k = -\frac{E_a}{RT} + \ln P, \quad (6)$$

where k is the rate constant, A is the Arrhenius constant, E_a is the activation energy (J mol^{-1}), R is the gas constant (8.314 J JK^{-1}mol^{-1}), and T is the absolute temperature (K). The slope of the graph plotted between ln k vs. $1/T$ represents the E_a/R value. Here, h = Planck's constant (6.626×10^{-34} J.s), and k_b = Boltzmann's constant (1.38×10^{-23} JK^{-1}).

2.7. Heterogeneity Test and Test for reusability. The heterogeneity of the catalyst was tested using hot Sheldon's test [21], with the catalyst reaction being carried out for 40 min, followed by a catalyst-free reaction mixture for another 20 min, with the development of the reaction being tracked using thin-layer chromatography.

Recyclability is one of the economical applications for the catalyst. To confirm the catalyst's reusability test, *J. curcas* oil was transesterified using a recycled catalyst under optimal reaction conditions; after the transesterification reaction was completed the catalyst was removed by filtration method using Whatman filtration, and it was washed with methanol and hexane. Then, the catalyst was dried overnight at 80°C. Before the reuse of the catalyst, it was measured.

3. Results and Discussions

3.1. Total Acidity Test Using Boehm Titration. The catalyst of 100 mg was dissolved in 40 mL of 0.05 M NaOH and stirred for 24 hr. The mixture was then filtered, and 10.00 mL of aliquot was taken and acidified with 20.00 mL of standardized 0.05 M HCl solution. Further, phenolphthalein indicator was added and titrated with standardized 0.05 M NaOH. The same procedure was repeated to get the concordant value. Using Equation (1), the total acidity of LP-1, LP-2, and LP-3 was calculated to be 2.01, 2.42, and 0.92 mmol g^{-1}.

3.2. Catalyst Characterization

3.2.1. Surface Area and Mean Pore Size of Synthesized Compound. The impact of $ZnCl_2$ dosage at 500°C carbonization temperature on the product structure was examined through N_2 adsorption–desorption techniques. The impregnation ratio has emerged as a crucial factor in the synthesis of activated carbon through chemical activation. $ZnCl_2$ intensifies the breakdown of structures within the carbon-containing raw materials. Consequently, during carbonization, dehydration of the biomass takes place, leading to charring, aromatization of the carbon skeleton, and the formation of the porous structure [22, 23]. Figures 3(a), 3(b), and 3(c) represent the BET isotherm profile, which shows a typical Type-1 adsorption isotherm accompanied with H4 hysteresis loops where there are steep increase and limited uptake of N_2 at lower relative pressure (p/p_0), followed by a more modest increment in adsorption as the pressure continues to increase [24]. Thus the activated carbons for different impregnation ratios (LP-1, LP-2, and LP-3), suggest presence of both microporosity and mesoporosity [25] (Figures 3(d), 3(e), and 3(f)).

Table 1 outlines the impact of different $ZnCl_2$ impregnation proportions on the texture and porosity of the carbonized biomass. An uptake in the $ZnCl_2$ impregnation ratio from 1 : 1 to 1 : 2 results in a nominal enhancement of both the surface area and the volume of mesopores, indicating that a moderate $ZnCl_2$ presence aids pore formation in the carbon matrix [22]. Nonetheless, escalating the ratio to 1 : 3 causes a marked decline in surface area and micropore volume. Such patterns are in line with the dual function of $ZnCl_2$ as a dehydration and activation agent during carbonization. At low ratios, $ZnCl_2$ effectively etches the biomass, increasing its porosity, surface area, and mesoporosity. However, at an excessive impregnation level of 1 : 3, the surplus of $ZnCl_2$ provokes a structural collapse that obstructs micropores, thereby restraining both surface outreach and microporosity. Mesoporosity initially scales up owing to the ideal etching activity but later diminishes with the over-etching at the ZnCl2 ratio of 1 : 3. These dynamics showcase an optimal concentration of $ZnCl_2$ that bolsters porosity, whereas surpassing this limit may prevent pore development, undermining the preferable attributes of the activated carbon [22].

3.2.2. Structural and Morphological Study of the Prepared Samples Using SEM EDX Analysis. The successful incorporation of sulfur into the activated carbon was confirmed through energy-dispersive X-ray spectroscopy analysis. Figures 4(d), 4(e), and 4(f) display the EDX spectra for the specific regions indicated in the SEM images of Figures 4(a), 4(b), and 4(c) for synthesized compound LP-1, LP-2, and LP-3, respectively. Additionally, Figures 4(g), 4(h), and 4(i) exhibit the breakdown of elemental constituents for each

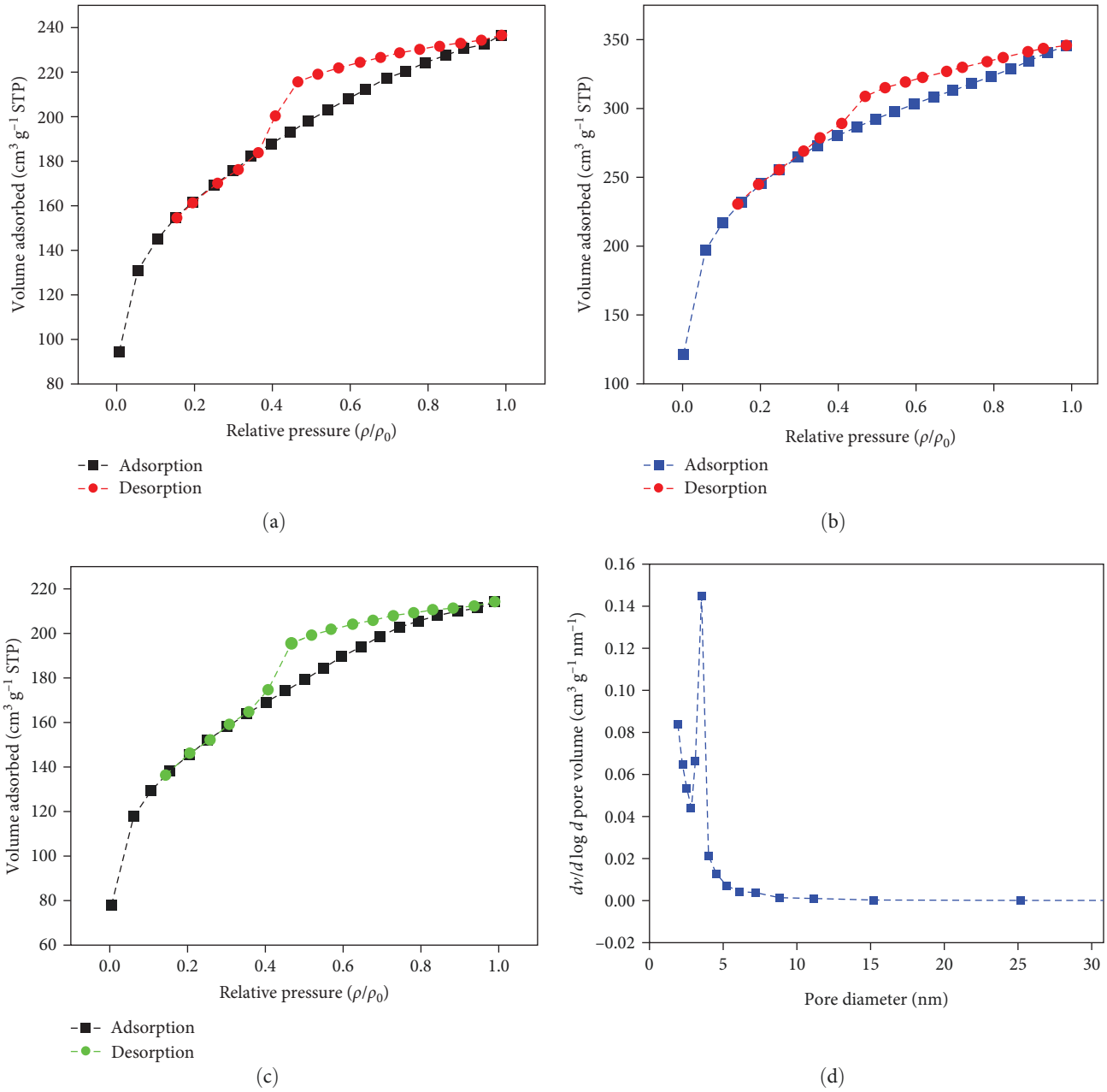


Figure 3: Continued.

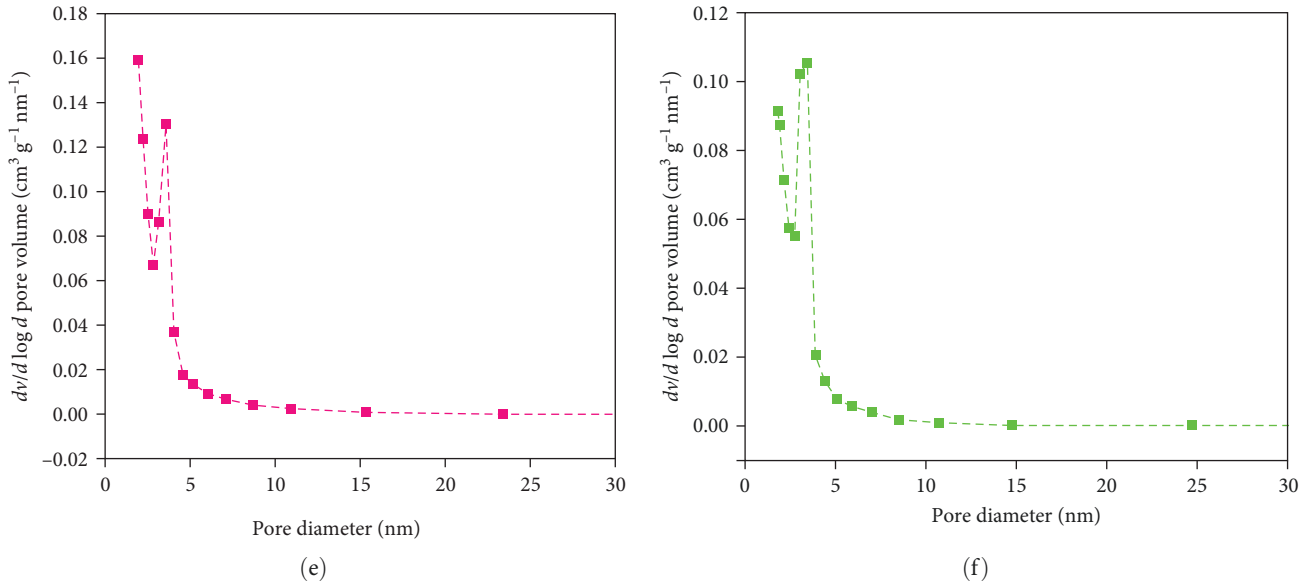


FIGURE 3: N_2 adsorption–desorption isotherm of synthesized compound LP-1 (a), LP-2 (b), and LP-3 (c). BJH pore size distribution curve of LP-1 (d), LP-2 (e), and LP-3 (f) compound.

TABLE 1: Comparison of surface area, pore size, and volume of BET result along with EDX data of the prepared samples.

AC : $ZnCl_2$ impregnation ratio	Surface area (m^2 g^{-1})	Pore size (nm)	Pore volume (cc g^{-1})	
			Mesoporous	Microporous
1 : 1	512.08	3.51	0.21	0.08
1 : 2	**863.09**	**1.90**	**0.30**	**0.14**
1 : 3	572.3	3.50	0.20	0.09

Bold signifies that the 1 : 2 impregnation ratio is the catalyst of the current manuscript, showing its superior properties.

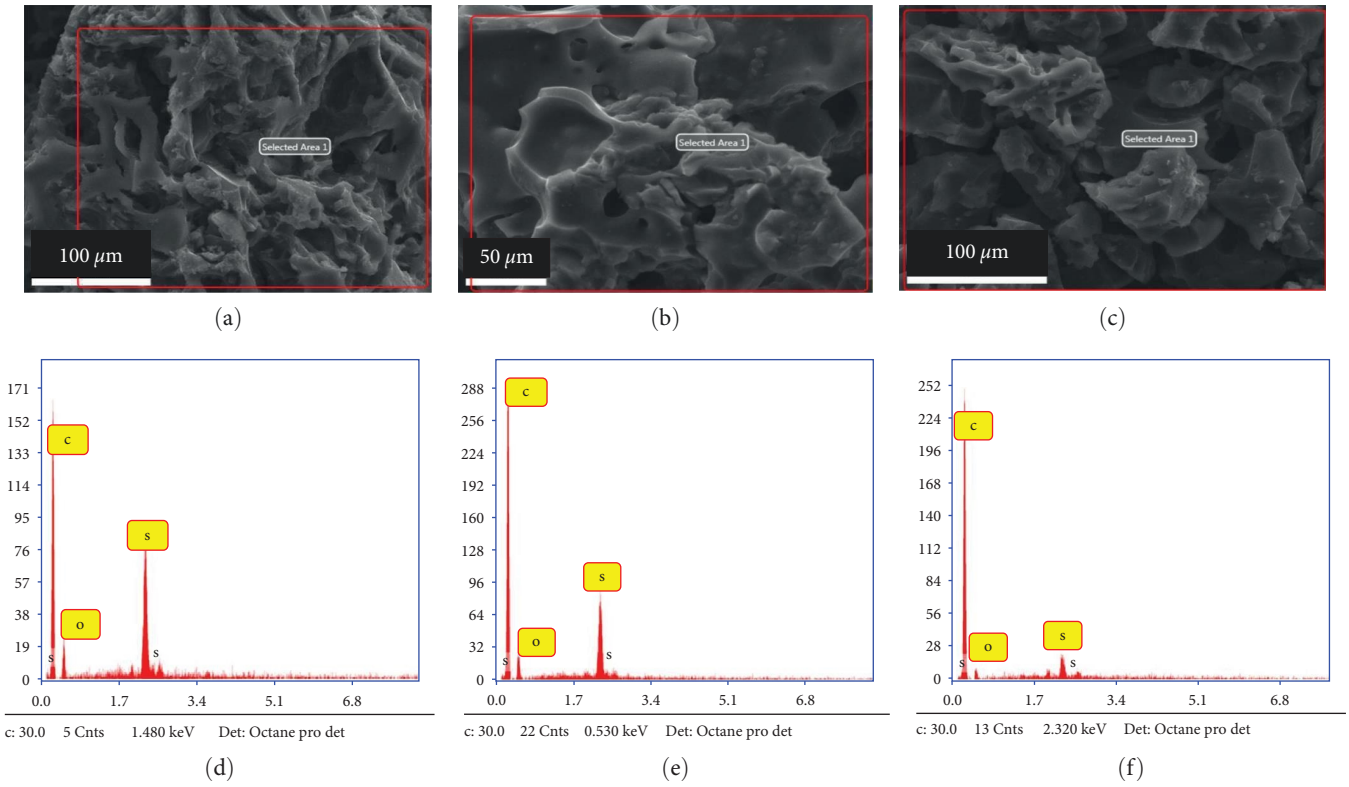


FIGURE 4: Continued.

Elements	Weight %	Atomic %
C	77.32	83.95
O	16.71	13.62
S	5.98	2.43

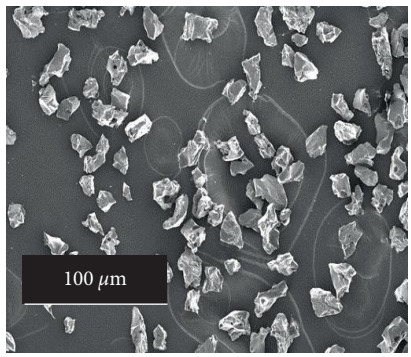
(g)

Elements	Weight %	Atomic %
C	80.26	85.78
O	15.72	12.61
S	4.02	1.61

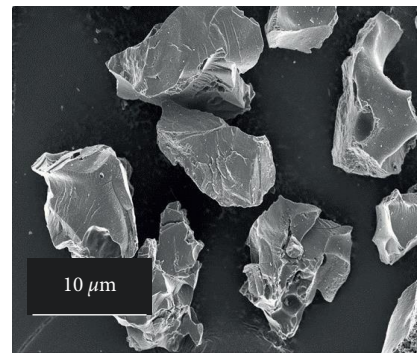
(h)

Elements	Weight %	Atomic %
C	89.58	92.34
O	9.38	7.26
S	1.04	0.40

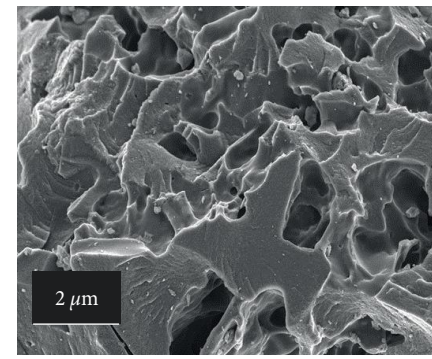
(i)



(j)



(k)



(l)

FIGURE 4: EDX spectrum (d), (e), and (f) for red box area of the image (a), (b), and (c) and its EDX data (g), (h), and (i) of LP-1, LP-2, and LP-3 compound. Scale bars 100 μm (a), 50 μm (b), and 100 μm (c). Representative SEM micrographs of LP-2 catalyst (j), (k), and (l). Scale bars 100 μm (j), 10 μm (k), and 2 μm (l).

synthesized material LP-1, LP-2, and LP-3. The EDS data lead us to deduce that there is a decline in the percentage weight of sulfur as the ratio of $ZnCl_2$ increases from 1 : 1 to 1 : 3.

The activated carbon compound known as LP-2, which contains a sulfur content of 4.02 wt.%, delivered a significantly higher yield of biodiesel (95.2% ± 0.4%) compared to LP-1 (80.1% ± 0.4%) with a sulfur content of 5.98 wt.%. This increase in yield can be linked to the enhanced specific surface area of LP-2 at 863 m^2 g^{-1}, which amplifies the number of active catalytic sites (COOH, OH, and SO_3H), along with a greater pore volume of 0.30 cc g^{-1} that promotes effective mass transfer as well as even distribution of mechanical forces and thermal energy during the transesterification process. Consequently, the activated carbon that was impregnated with a $ZnCl_2$ ratio of 1 : 2 and subsequently functionalized to introduce sulfonated species was identified as the catalyst for further transesterification.

SEM image of the LP-2 catalyst is shown in Figures 4(j), 4(k), and 4(l). It reveals that the catalyst contains a porous carbon network structure and surface property, which is composed of various kinds of random fragments, the clustering of which is made of graphitized carbon, the explanation for which lies in the removal of water during the carbonization process [26].

3.2.3. XRD, FTIR, and TGA Analysis of LP−2 Catalyst. The XRD patterns (Figure 5(a)) of the LP-2 catalyst show a prominent peak in the 20°–30°, 2θ range, which corresponds to the (002) plane of the material derived from carbonized lemon peel under JCPDS file no. 41-1487 [27]. These results validate the efficient carbonization of lemon peel, with the broad peak attributed to amorphous carbon sheets that are randomly oriented [28]. The detection of specific peaks associated with different functional groups in the LP-2 catalyst was studied through FTIR analysis (Figure 5(b)). Here, the observation of a peak at 1,163 cm^{-1} indicates the symmetric stretching of S═O [6]. Additionally, the presence of C—H stretching and carbonyl stretching (C═O) in aromatic rings was evidenced by the formation of peaks at 606 and 1,591 cm^{-1} [29], respectively. Furthermore, a broad absorption at 3,248 cm^{-1} was noted, indicating the occurrence of O—H stretching [14], with this peak generally being most prominent in lower-temperature samples. Figure 5(c) shows the results of the LP-2 catalyst's thermogravimetric analysis conducted between 50 and 900°C. According to the data, the LP-2 catalyst experienced an initial mass loss of approximately 9% between 30 and 90°C, primarily due to the removal of adsorbed water [6]. The catalyst remained stable up to 320°C, after which a 5% mass loss occurred, attributed to the decomposition of functional groups [30]. Beyond 400°C, further mass loss was observed due to the release of compounds such as CO and CO_2 [31]. The catalyst exhibited stability beyond 800°C.

3.2.4. Characterization of FAME. The impact of the MeOH: JCO molar ratio on the transesterification reaction depicted in (Figure 6(a)) was examined by varying the ratio from 1 : 5 to 1 : 25, with an 8 wt.% loading of catalyst, at 100°C for 60 min. As anticipated, the forward drive of the equilibrium was initially facilitated by excess MeOH upon increasing the molar ratio. The highest JCO yield (95.2% ± 0.4%) was observed when the JCO: MeOH ratio was 1 : 20. However, as more MeOH was introduced, leading to the dilution of the

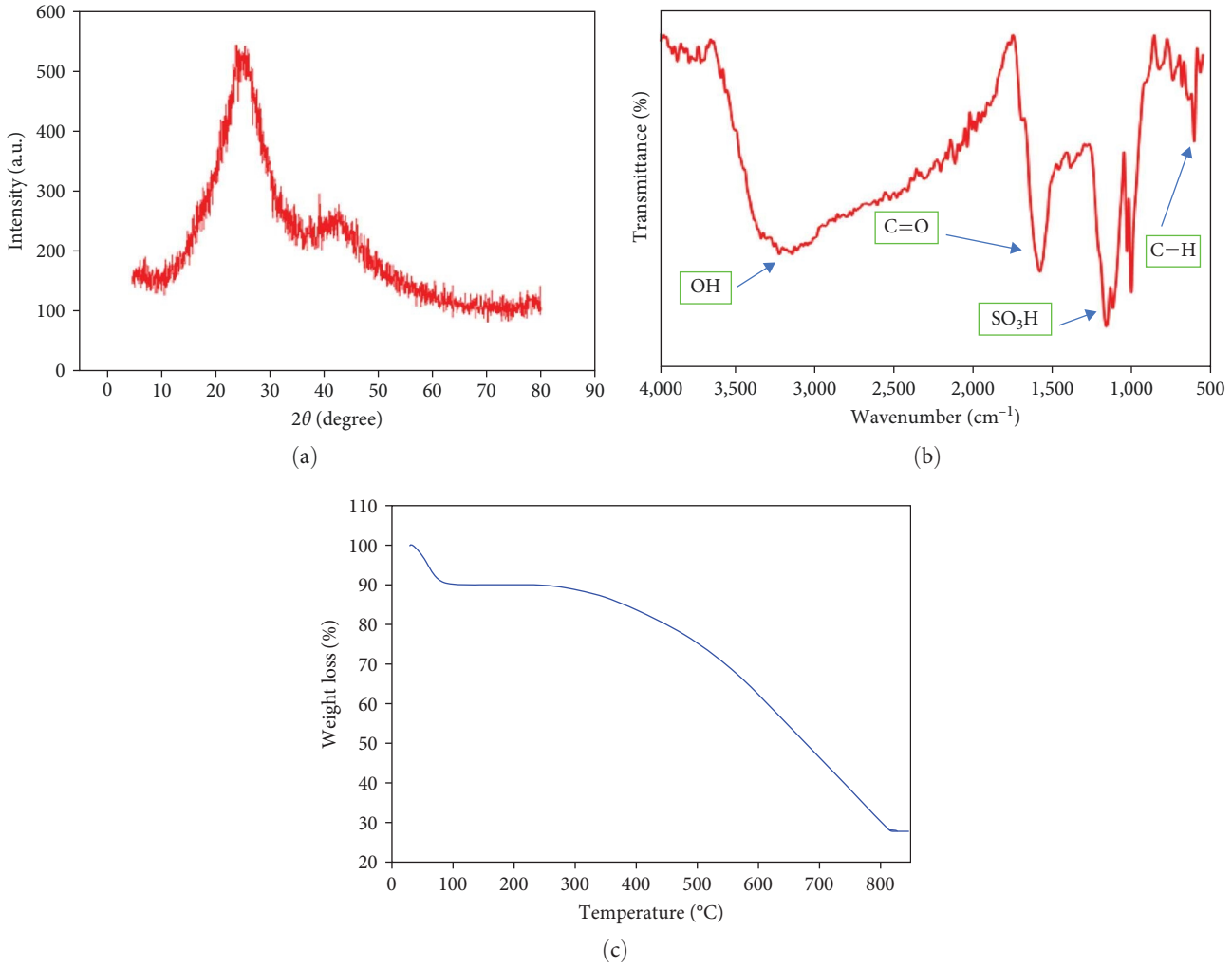


Figure 5: XRD pattern (a), FTIR spectrum (b), and TGA graph (c) of LP-2 catalyst.

reaction mixture and potentially allowing more water to enter the system and drive the reverse reaction [32], the yield decreased with further increments in the molar ratio.

The impact of catalyst loading on transesterification in a 1 : 20 JCO : MeOH ratio at 100°C for 60 min was investigated by adjusting the loading from 2 to 10 wt.% (Figure 6(b)). With the increase in catalyst amount, yield rose from 2 to 8 wt.% as more active sites became available. The reason for the observed maximum yield at 8 wt.% of catalyst and the lack of further increase at 10 wt.% was attributed to an increase in viscosity, which impeded reagent diffusion to the catalyst active site [33, 34].

The transesterification of JCO through the use of a catalyst involves a three-phase system (MeOH, catalyst, and oil), underscoring the significance of temperature in controlling reagent access to active sites. The impact of temperature on the transesterification reaction was varied between 70 and 110°C (Figure 6(c), JCO : MeOH 1 : 20, 8 wt.% catalyst, 60 min were kept constant). For an endothermic process, the yield increased as the temperature was raised. On the other hand, biodiesel yield decreased above 100°C, which was linked to MeOH evaporation [35, 36].

Using JCO:MeOH 1 : 20, 8 wt.% catalyst, and 100°C, the reaction was finally monitored over time ranges between 30 and 70 min (Figure 6(d)). Biodiesel yield reached just 74.1% ± 0.3% after 30 min but jumped to 95.2% ± 0.4% in 60 min. However, extending the reaction time to 70 min did not significantly affect the yield, possibly because the reaction had reached equilibrium [37]. Lastly, after studying the reaction parameter, the following reaction conditions (JCO:MeOH 1 : 20, 8 wt.%, catalyst, 100°C, 70 min) were considered as the optimized reaction parameter for our current work.

3.2.5. Analysis Using NMR, GC–MS Spectra, and FTIR of Product Biodiesel. NMR spectroscopy of the product was performed, as shown in Figure 7. In the ^{1}H NMR spectra of biodiesel, characteristic methoxy protons peak was obtained at 3.64 ppm subsequent to the methoxy protons in the methyl ester, confirming the successful formation of FAME. ^{1}H NMR revealed 97.41% conversion of biodiesel using Equation (3).

In this study, GC–MS analysis was conducted on the resulting product, revealing the presence of eight components. The reaction, conducted at 100°C for 60 min, with 8 wt.% catalyst and a 1 : 20 molar ratio of JCO :MeOH confirmed a

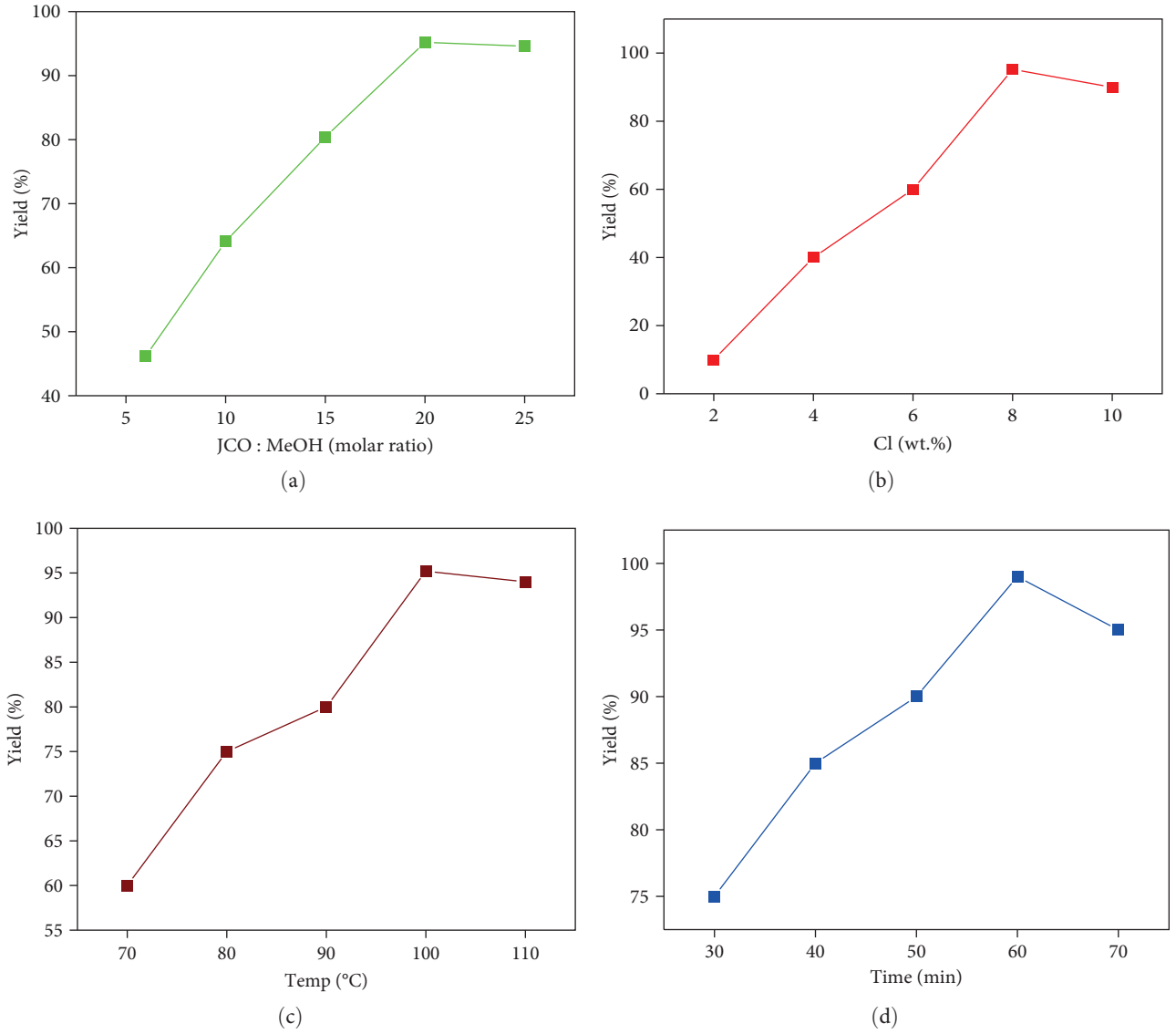


Figure 6: Optimization of FAME using different parameters (a) molar ratio (at 100°C, 1 hr, 8 wt.% catalyst loading), (b) catalyst loading (at 100°C, 1 hr, 20 mol/mol ratio of MeOH to JCO), (c) reaction temperature (at 1 hr, 20 mol/mol ratio of MeOH to JCO, 8 wt.% catalyst loading), and (d) reaction time (at 100°C, 20 mol/mol ratio of MeOH to JCO, 8 wt.% catalyst loading).

high biodiesel yield of 95.2% ± 0.4%. The major components were 9-octadecenoic acid (Z)-, methyl ester (C18 : 1,44.8%), Hexadecanoic acid, methyl ester (C16 : 0,12.5%) and Linoleic acid ethyl ester (C18 : 2,15.1%). The methyl esters of various acid constituents are represented (Figure 8) as C16 : 0, C18 : 2, C18 : 3, and C18 : 0 and C21 : 1, C21 : 0, and C22 : 0, respectively, on the total ion chromatogram. Table 2 presents the various components' numerical values.

The biodiesel product was analyzed using FTIR to identify its functional groups comparison was made between the biodiesel product and JCO, as depicted in Figure 9. Both spectra exhibited numerous absorption bands of similar intensity, attributed to the shared chemical properties TG and esters [10]. The stretching vibration of C—H was evidenced by absorption bands at 2,931 and 2,856 cm^{-1} [10]. Additionally, characteristic absorption bands around 1,749 and 1,176 cm^{-1} corresponded to the stretching vibrations of C═O ester and C—O ester, respectively [6]. Both JCO and biodiesel spectra displayed a peak at 1,481 cm^{-1}, indicative of O—CH_3 deformation vibration. The formation of biodiesel from JCO was confirmed by new peaks observed at 1,031 cm^{-1}, which were attributed to stretching vibrations of C—O (esters). Finally, a peak at 726 cm^{-1} was observed due to the overlapping of CH_2 vibrations, similar to peaks observed in JCO feedstocks [6].

3.3. Kinetic Study of Transesterification. The kinetic study examined the transesterification of JCO catalyzed by LP-2 catalyst at varying temperatures (70–100°C). It has been previously reported that the transesterification of TGs proceeds according to pseudo-first-order kinetics when there is an excess of alcohol present [38]. The corresponding graphs between −ln (1−X) vs. time display the expected linear relationship in Figure 10(a), respectively. Pre-exponential

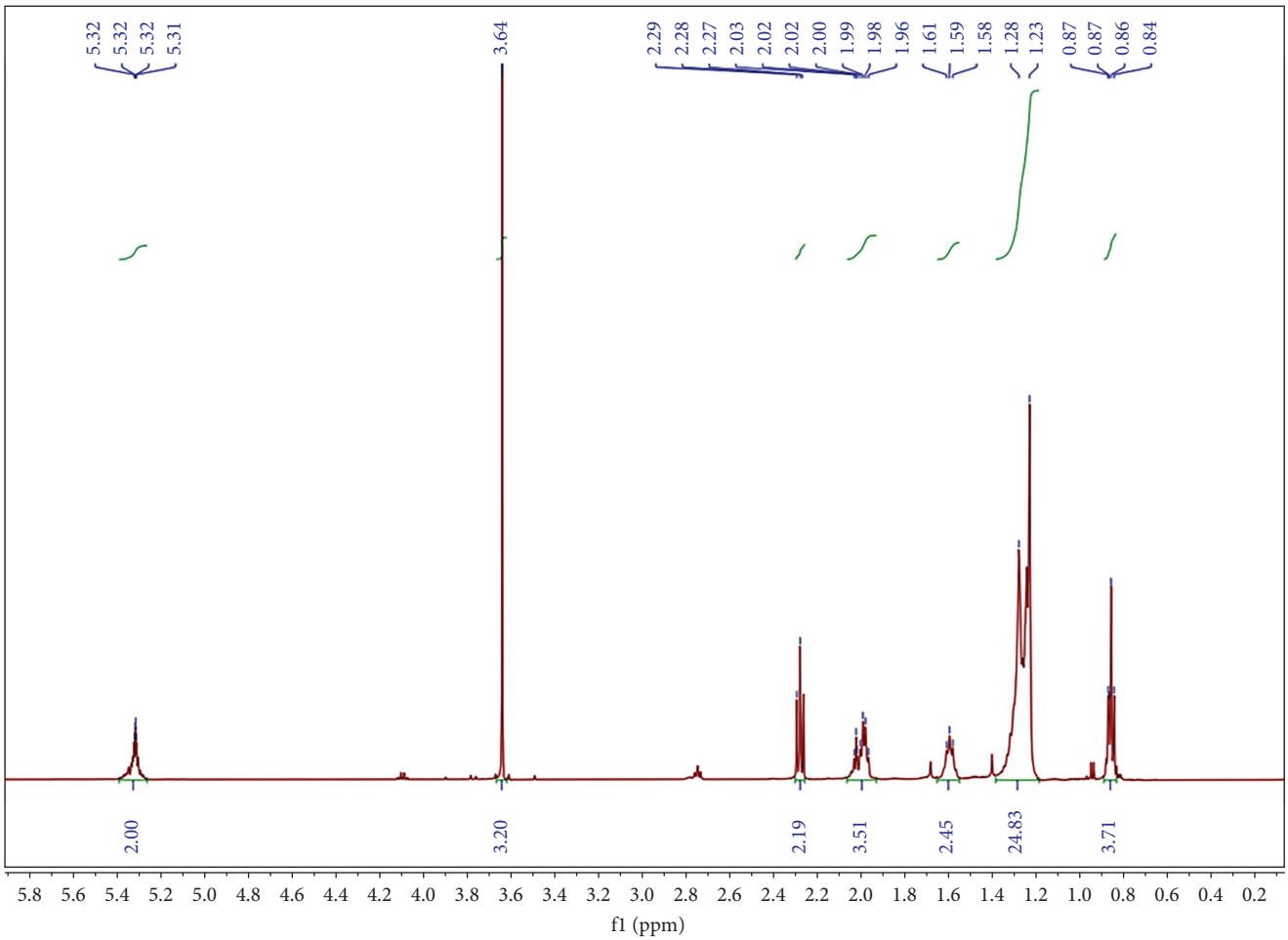


Figure 7: ^{1}H-NMR spectra of the product after transesterification.

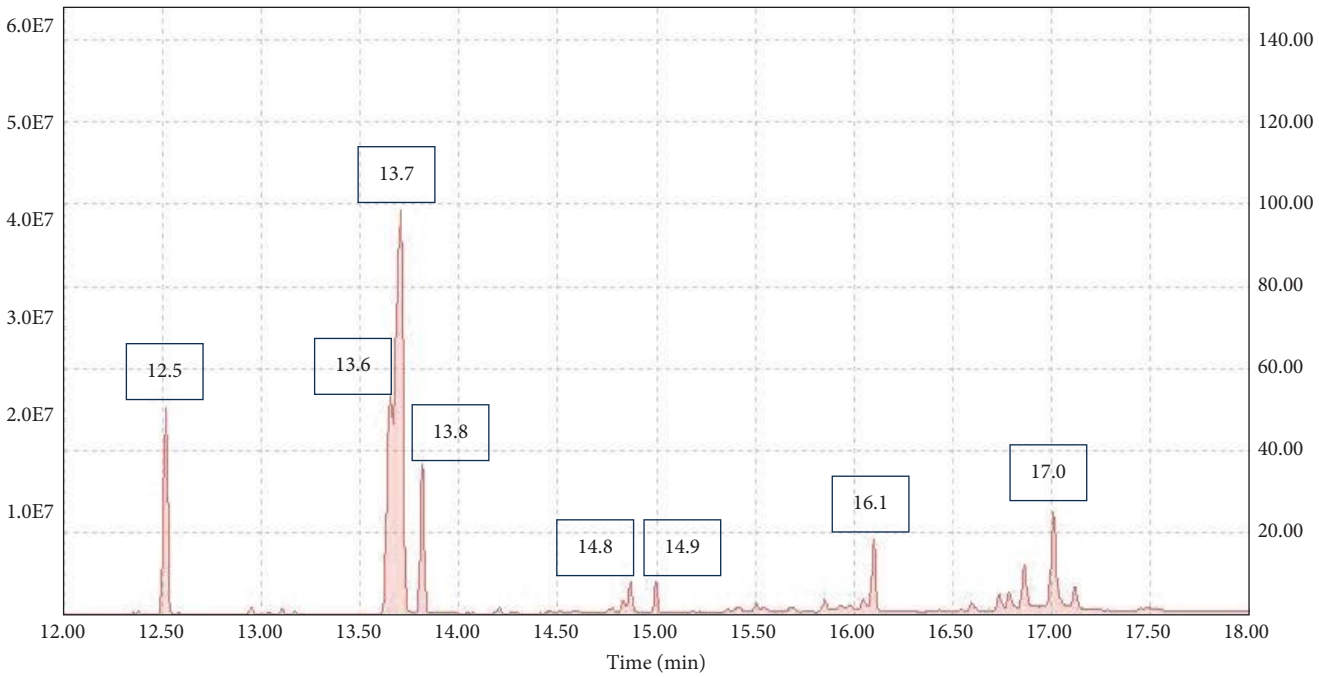


Figure 8: GC–MS spectra of the product biodiesel.

Table 2: Chemical composition of product JCO biodiesel.

Peak no.	Component name	Retention time (mins)	Corresponding acid	Proportion (%)
1	Hexadecanoic acid, methyl ester	12.5	C16 : 0	12.5
2	Linoleic acid ethyl ester	13.6	C18 : 2	15.1
3	9-Octadecenoic acid (Z)-, methyl ester	13.7	C18 : 1	44.8
4	Octadecanoic acid, methyl ester	13.8	C18 : 0	8.6
5	cis-Methyl 11-eicosanoate	14.8	C21 : 1	2.3
6	Methyl 18-methylnonadecanoate	14.9	C21 : 0	2.1
7	Docosanoic acid, methyl ester	16.1	C22 : 0	4.8
8	9-Octadecenoic acid (Z)-, 2,3-dihydroxypropyl ester	17.0	C21 : 0	9.5

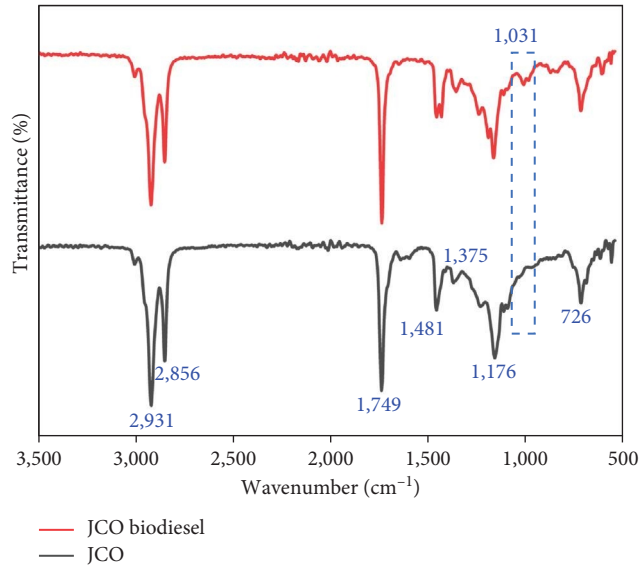


Figure 9: FTIR spectra comparison of JCO and JCO biodiesel.

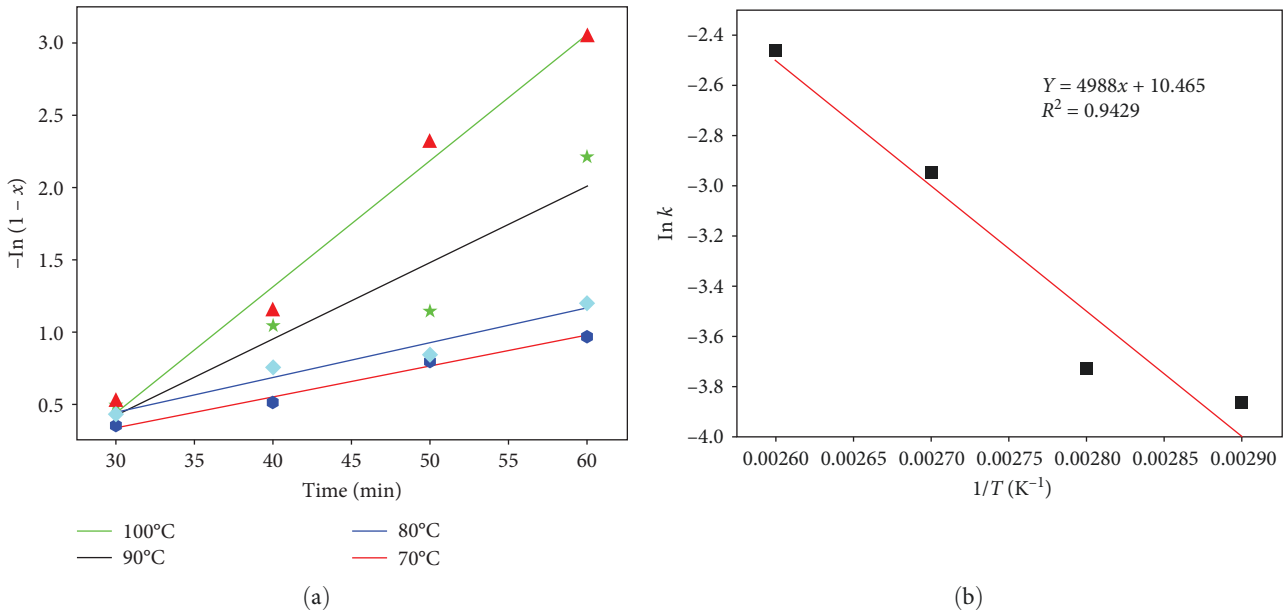


Figure 10: Kinetic study of LP-2 catalyst shows (a) plot of $-\ln(1-x)$ vs. time (min) and (b) corresponding plot of $\ln k$ vs. $1/T$ (K^{-1}).

Table 3: Comparison of performance of catalyst with previously reported catalyst using JCO feedstock.

Entry	Catalyst	Conditions[a]	TOF[c] (mol g^{-1} hr^{-1})	CRC (Y)	Yield (%)	Ref
1	Sr^{2+}-CaO/MgO	9 : 1, 5, 65, 120	0.011	4 (90.00)	99.00	[40]
2	ZnO/γ-Al_2O_3	1 : 40, 10, 300, 3	0.003	6 (95.16)	95.64	[41]
3	Waste ox bone	12 : 1, 5, 338, 240	0.005	3 (90.00)	96.82	[42]
4	ZnO-CFA	11.8 : 1, 1.63, 60.4, 180	0.032	3 (91.08)	86.75	[43]
5	ZnO	18 : 1, 1.5, 67, 100	0.001	4 (98.00)	98.00	[44]
6	MPD-SO_3H-IL	50 : 1, 6, 160, 8	0.002	4 (74.00)	94.00	[45]
7	CaO-NiO	15 : 1, 5, 65, 360	0.002	6 (80.00)	80.00	[46]
8	AC-600-SO_3H@Fe/C	25 : 1, 10, 200, 5	0.002	4 (74.00)	94.00	[47]
9	Zn8@Fe-C400	40 : 1, 7, 160, 4	6.43	10 (94.30)	100.0	[48]
10	CaO-La_2O_3	24 : 1, 3, 160, 3	0.012	5 (60,00)	99.00	[49]
11	CaMgO	15 : 1, 4, 65, 6	0.003	4 (80.00)	80.00	[50]
12	Mg—Al HT	30 : 1, 10, 120, 120	0.004	5 (90.00)	75.00	[51]
13	Musa Champa	9 : 1, 5, 65, 10	0.002	3 (93.79)	98.27	[52]
14	LP-2	1 : 20, 8, 100, 60[b]	0.013	7 (88.4)	95.2% ± 0.4%	Present work

[a]JCO : MeOH molar ratio, catalyst loading (wt.%), temperature (°C), time (min). [b]Microwave heating. [c]TOF (mol g^{-1} hr^{-1}) = moles of biodiesel converted per gram of catalyst per hour. CRC (Y) = catalyst reusability cycles (yield %).

component and activation energy (E_a) were identified from the slope and intercept of the $-\ln k$ vs. $1/T$ plot shown in Figure 10(b). The obtained activation energy for the pseudo-first-order kinetics was calculated as 41.47 kJ mol^{-1}, while the pre-exponential factor was found to be 3.5×10^4 min^{-1}. Notably, this E_a value aligns well with previously reported values ranging from 24.7 to 84.1 kJ mol^{-1} [39].

3.4. Comparison of Performance of LP-2 Catalyst with Previously Reported Catalyst Using JCO as Biodiesel Feedstock. The current LP-2 catalyst synthesized from lemon peel has been compared with previously reported heterogeneous catalysts applied for the conversion of JCO to biodiesel in Table 3. Among the reported catalysts, ZnO-CFA [43] and CaO-NiO [46] require longer reaction times for the production of biodiesel when compared to other catalysts in Table 3. Meanwhile, catalysts like ZnO/γ-Al_2O_3 [41], MPD-SO_3H-IL [45], and AC-600-SO_3H@Fe/C [47] require higher reaction temperatures for the transesterification reaction, as can be seen in Table 3. Under our study, the performance of the present LP-2 catalyst reported a high 95.2% ± 0.4% biodiesel yield despite using a lower catalyst loading than the catalysts such as Mg—Al HT [51] and ZnO/γ-Al_2O_3 [41]. Furthermore, industrial chemists typically view turnover frequency, or TOF, as the most crucial indicator for evaluating catalyst activity. The TOF for our current work was determined to be 0.013 mol g^{-1} hr^{-1}, which is higher than most of the catalysts listed in Table 3, such as waste ox bone [42], CaMgO [50], Sr^{2+}-CaO/MgO [40], ZnO/γ-Al_2O_3 [41], Mg—Al HT [51], ZnO [44], CaO-NiO [46] except ZnO-CFA [43] and Zn8@Fe-C400 [48], which can be compensated by current catalyst low activation energy. Finally, the LP-catalyst shows a greater recyclability than many of the reported catalysts, and hence, it can be considered a sustainable contribution to the sustainability of the biodiesel industry.

$$\text{TOF} = \frac{\%\ \text{conversion of JCO}}{(\text{time})\ (\text{catalyst wt.}\%)\ (\text{molar mass of JCO})}. \tag{7}$$

3.5. Heterogeneity Test and Catalyst reusability Operation. Confirmation of the catalyst's heterogeneity was achieved using the Hot Sheldon filtration method. After 40 min, the catalyst was removed from the reaction mixture, resulting in the production of 85% ± 0.2% biodiesel (Figure 11(a)). Subsequently, without the catalyst, the reaction continued for an additional 20 min, yielding 87.1% biodiesel. This represented a 2.1% ± 0.2% increase in yield. The outcome substantiated the maintenance of the catalyst's heterogeneity, as trace amounts remained in the reaction mixture, leading to the observed enhancement in biodiesel yield from JCO.

The recyclability of the LP-2 catalyst was conducted under the previously optimized condition, shown in Figure 11(b). After each cycle, the catalyst was removed from the reaction mixture using the Whatman filter paper, thoroughly cleaned with methanol and hexane (2 x 15 mL), and then dried in an oven at 80°C for an overnight, after which the catalyst was weighed and reused. The catalytic activity dropped within seven runs, going from 95.2% ± 0.4% to 88.4% ± 0.6%, which was attributed to the leaching of active sites as confirmed by SEM EDX analysis (Figures 11(c) and 11(d)), the result is supported by other reported literature as well [3, 53, 54]. After seven cycles, EDS analysis revealed a notable reduction in sulfur content to 2.93 wt.% Figure 11(d) from its initial value of 4.02 wt.% (Figure 4(h)).

4. Conclusion

In this work, the effect of carbon-based acidic catalysts for biodiesel production from feedstocks derived from *J. curcas*

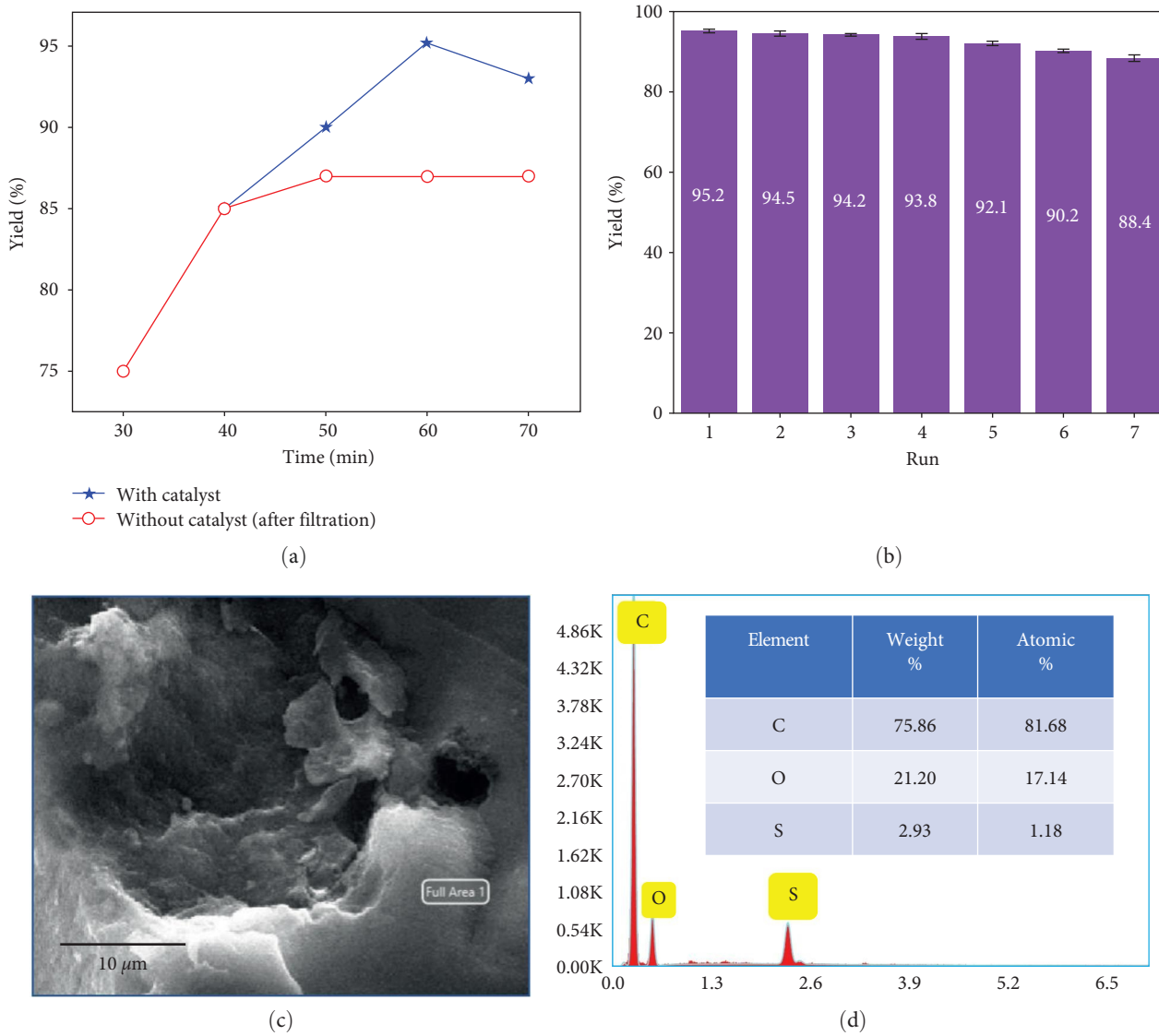


FIGURE 11: (a) Heterogeneity test of LP-2 catalyst in transesterification recation, (b) reusability test of LP-2 catalyst over seven reaction cycles, (c) SEM image, and (d) EDX spectra of LP-2 catalyst after seven reaction cycles.

oil was investigated. Several analyses, including FTIR, BET, XRD, SEM-EDS, TGA, and GC–MS, were performed to investigate the catalyst. The presence of highly porous acidic carbonaceous material was attributed to the catalyst's high catalytic activity. The reusability of the catalyst was also looked into for potential future uses. A kinetic study returned an activation energy of 41.47 kJ mol^{-1}, which is at the lower end of the normal range for comparable reactive systems in the literature, and a correspondingly impressive TOF of 0.013 mol g^{-1} hr^{-1}. The catalyst's reusability tests revealed a decline in the yield (88.4%) after the seventh cycle. To prevent the leaching of active sites, it is recommended to increase the hydrophobicity of the catalyst. This can be achieved by preventing water desorption on the surface and maintaining high acid concentrations. Finally, the green synthesis-activated biochar-derived biodiesel offers a practical and environmentally beneficial replacement for conventional fossil fuels.

Abbreviations

DI:	Deionized water
TGs:	Triglycerides
JCO:	*Jatropha curcas* oil
BDS:	Benzene diazonium sulfonate
SEM:	Scanning electron microscopy
FAMEs:	Fatty acid methyl esters
NMR:	Nuclear magnetic resonance
FTIR:	Fourier-transform infrared spectroscopy
XRD:	X-ray powder diffraction
JCO : MeOH:	*Jatropha curcas* oil : methanol
AC-600-SO3H@Fe/C:	Activated carbon-600- SO3H@Fe/C
FFA:	Free fatty acids
MPD-SO3H-IL:	Mesoporous polymer-sulfonic acid-ionic liquid

AC:	Activated carbon
SEM-EDS:	Scanning electron microscopy-energy dispersive spectroscopy
BET:	Brunauer–Emmett–Teller
GC–MS:	Gas chromatography–mass spectroscopy.

Data Availability

Data will be made available upon request.

Conflicts of Interest

There are no conflicts to report.

Authors' Contributions

Supongsenla Ao and Sudeshna Ghorui contributed equally to this work by conducting the conceptualization, methodology, investigation, data analysis, and writing the original draft. Hui Li conducted the formal analysis and reviewed the paper. Gurunathan Baskar reviewed and edited the paper. Samuel Lalthazuala Rokhum conceptualized and supervised the paper. The published version of the manuscript has been read and agreed to by all authors.

Acknowledgments

This work is funded by the Science and Engineering Research Board (SERB), India (grant no. EEQ/2023/000336) and the Council of Scientific and Industrial Research (CSIR), India (grant no. 01/3099/23/EMR-II). We acknowledge the CIF NIT Silchar, SAIFs (IIT Bombay, IIT Patna), and CSIR IIM-Jammu for analysis.

References

[1] S. Das, J. M. H. Anal, P. Kalita, L. Saikia, and S. L. Rokhum, "Process optimization of biodiesel production using waste snail shell as a highly active nanocatalyst," *International Journal of Energy Research*, vol. 2023, Article ID 6676844, 26 pages, 2023.

[2] S. H. Y. S. Abdullah, N. H. M. Hanapi, A. Azid et al., "A review of biomass-derived heterogeneous catalyst for a sustainable biodiesel production," *Renewable and Sustainable Energy Reviews*, vol. 70, pp. 1040–1051, 2017.

[3] S. P. Gouda, J. M. H. Anal, P. Kumar, A. Dhakshinamoorthy, U. Rashid, and S. L. Rokhum, "Microwave-assisted biodiesel production using UiO-66 MOF derived nanocatalyst: process optimization using response surface methodology," *Catalysts*, vol. 12, no. 11, Article ID 1312, 2022.

[4] Y. Idrissou, T. Mazari, S. Benadji, M. Hamdi, and C. Rabia, "Homogeneous and heterogeneous sunflower oil methanolysis over 12-tungstophosphoric, sulfuric and boric acids," *Reaction Kinetics, Mechanisms and Catalysis*, vol. 119, no. 1, pp. 291–304, 2016.

[5] Y. H. Tan, M. O. Abdullah, J. Kansedo, N. M. Mubarak, Y. S. Chan, and C. Nolasco-Hipolito, "Biodiesel production from used cooking oil using green solid catalyst derived from calcined fusion waste chicken and fish bones," *Renewable Energy*, vol. 139, pp. 696–706, 2019.

[6] S. Ao, S. P. Gouda, M. Selvaraj et al., "Active sites engineered biomass-carbon as a catalyst for biodiesel production: process optimization using RSM and life cycle assessment," *Energy Conversion and Management*, vol. 300, Article ID 117956, 2024.

[7] S. Ao, M. V. L. Chhandama, H. Li, and S. L. Rokhum, "Microwave-assisted sustainable production of biodiesel: a comprehensivereview," *Current Microwave Chemistry*, vol. 10, pp. 3–25, 2023.

[8] A. F. Lee, J. A. Bennett, J. C. Manayil, and K. Wilson, "Heterogeneous catalysis for sustainable biodiesel production *via* esterification and transesterification," *Chemical Society Reviews*, vol. 43, no. 22, pp. 7887–7916, 2014.

[9] S. Ao and S. L. Rokhum, "Recent advances in the valorization of biodiesel by-product glycerol to solketal," *Journal of Chemistry*, vol. 2022, Article ID 4938672, 18 pages, 2022.

[10] A. Das, B. Khumbharkar, P. Pachfule et al., "Sheet-like superparamagnetic biochar-based acid catalyst for biodiesel production: process optimization, kinetics, thermodynamics, and life cycle cost analysis," *Process Safety and Environmental Protection*, vol. 189, pp. 94–910, 2024.

[11] B. Chen, Z. Zhou, Y. Li et al., "Catalytic pyrolysis of fatty acids and oils into liquid biofuels and chemicals over supported Ni catalysts on biomass-derived carbon," *Applied Catalysis B: Environment and Energy*, vol. 338, Article ID 123067, 2023.

[12] B. Maleki, Y. Kalanakoppal Venkatesh, S. Siamak Ashraf Talesh, H. Esmaeili, S. Mohan, and G. R. Balakrishna, "A novel biomass derived activated carbon mediated AC@ZnO/NiO bifunctional nanocatalyst to produce high-quality biodiesel from dairy industry waste oil: CI engine performance and emission," *Chemical Engineering Journal*, vol. 467, Article ID 143399, 2023.

[13] H. Choksi, S. Pandian, Y. H. Gandhi, and S. Deepalaxshmi, "Studies on production of biodiesel from madhuca indica oil using a catalyst derived from cotton stalk," *Energy Sources, Part A: Recovery, Utilization, and Environmental Effects*, vol. 43, pp. 3424–3433, 2021.

[14] S. Ao, U. Rashid, D. Shi et al., "Synthesis and utilization of biomass-derived sulfonated heterogeneous catalyst-BT-SO_3H for microalgal biodiesel production," *Environmental Research*, vol. 245, p. 118025, 2024.

[15] A. M. Oickle, S. L. Goertzen, K. R. Hopper, Y. O. Abdalla, and H. A. Andreas, "Standardization of the boehm titration: part II," *Method of Agitation, Effect of Filtering and Dilute Titrant*, vol. 48, no. 12, pp. 3313–3322, 2010.

[16] K. Malins, J. Brinks, V. Kampars, and I. Malina, "Esterification of rapeseed oil fatty acids using a carbon-based heterogeneous acid catalyst derived from cellulose," *Applied Catalysis A: General*, vol. 519, pp. 99–106, 2016.

[17] T. Maneerung, S. Kawi, Y. Dai, and C. H. Wang, "Sustainable biodiesel production via transesterification of waste cooking oil by using CaO catalysts prepared from chicken manure," *Energy Conversion and Management*, vol. 123, pp. 487–497, 2016.

[18] G. T. Ang, S. N. Ooi, K. T. Tan, K. T. Lee, and A. R. Mohamed, "Optimization and kinetic studies of sea mango (Cerbera odollam) oil for biodiesel production via supercritical reaction," *Energy Conversion and Management*, vol. 99, pp. 242–251, 2015.

[19] S. Ao and S. L. Rokhum, "Biomass derived heterogenous catalyst for synthesis of solketal from biodiesel byproduct glycerol," *Science Talks*, vol. 8, Article ID 100264, 2023.

[20] H. R. Harsha Hebbar, M. C. Math, and K. V. Yatish, "Optimization and kinetic study of CaO nano-particles catalyzed biodiesel production from Bombax ceiba oil," *Energy*, vol. 143, pp. 25–34, 2018.

[21] H. E. B. Lempers and R. A. Sheldon, "The stability of chromium in CrAPO-5, CrAPO-11, and CrS-1 during liquid phase oxidations," *Journal of Catalysis*, vol. 175, pp. 62–69, 1998.

[22] S. Yorgun, N. Vural, and H. Demiral, "Preparation of high-surface area activated carbons from paulownia wood by $ZnCl_2$ activation," *Microporous Mesoporous Mater*, vol. 122, pp. 189–194, 2009.

[23] A. N. A. El-Hendawy, S. E. Samra, and B. S. Girgis, "Adsorption characteristics of activated carbons obtained from corncobs," *Colloids and Surfaces A: Physicochemical and Engineering Aspects*, vol. 180, pp. 209–221, 2001.

[24] M. Thommes, K. Kaneko, A. V. Neimark et al., "Physisorption of gases, with special reference to the evaluation of surface area and pore size distribution (IUPAC technical report)," *Pure and Applied Chemistry*, vol. 87, pp. 1051–1069, 2015.

[25] R. Bardestani, G. S. Patience, and S. Kaliaguine, "Experimental methods in chemical engineering: specific surface area and pore size distribution measurements—BET, BJH, and DFT," *Canadian Journal of Chemical Engineering*, vol. 97, pp. 2781–2791, 2019.

[26] R. Liu, X. Wang, X. Zhao, and P. Feng, "Sulfonated ordered mesoporous carbon for catalytic preparation of biodiesel," *Carbon*, vol. 46, pp. 1664–1669, 2008.

[27] G. Y. Cui, C. Y. Wang, G. Q. Xiang, and B. Zhou, "An electrochemical sensor based on nitrogen doped carbon material prepared from nitrogen-containing precursors," *IOP Conference Series: Materials Science and Engineering*, vol. 292, 2018.

[28] S. Kang, J. Ye, Y. Zhang, and J. Chang, "Preparation of biomass hydrochar derived sulfonated catalysts and their catalytic effects for 5-hydroxymethylfurfural production," *RSC Advances*, vol. 3, no. 20, pp. 7360–7366, 2013.

[29] K. Tohdee, S. Semmad, A. Jotisankasa, P. Praserthdam, and B. Jongsomjit, "Investigation of sulfonated solid acid catalysts derived from oil palm kernel shell, corncob, and diatomaceous earth for esterification of ethanol and propanoic acid, characterisation and their performance," *Bioresource Technology Reports*, vol. 16, Article ID 100855, 2021.

[30] F. Jamil, S. K. Saxena, A. H. Al-Muhtaseb et al., "Valorization of waste "date seeds" bio-glycerol for synthesizing oxidative green fuel additive," *Journal of Cleaner Production*, vol. 165, pp. 1090–1096, 2017.

[31] H. M. Kefas, R. Yunus, U. Rashid, and Y. H. Taufiq-Yap, "Modified sulfonation method for converting carbonized glucose into solid acid catalyst for the esterification of palm fatty acid distillate," *Fuel*, vol. 229, pp. 68–78, 2018.

[32] A. N. Phan and T. M. Phan, "Biodiesel production from waste cooking oils," *Fuel*, vol. 87, no. 17-18, pp. 3490–3496, 2008.

[33] U. Rashid and F. Anwar, "Production of biodiesel through optimized alkaline-catalyzed transesterification of rapeseed oil," *Fuel*, vol. 87, no. 3, pp. 265–273, 2008.

[34] S. Ao, L. A. Alghamdi, T. Kress et al., "Microwave-assisted valorization of glycerol to solketal using biomass-derived heterogeneous catalyst," *Fuel*, vol. 345, Article ID 128190, 2023.

[35] L. C. Meher, V. S. S. Dharmagadda, and S. N. Naik, "Optimization of alkali-catalyzed transesterification of Pongamia pinnata oil for production of biodiesel," *Bioresource Technology*, vol. 97, no. 12, pp. 1392–1397, 2006.

[36] D. Leung, D. Yang, Z. Li, Z. Zhao, J. Chen, and L. Zhu, "Biodiesel from zophobas morio larva ol: process optimization and FAME characterization," *Industrial & Engineering Chemistry Research*, vol. 51, no. 2, pp. 1036–1040, 2012.

[37] V. Rossa, Y. D. S. P. Pessanha, G. C. Díaz, L. D. T. Câmara, S. B. C. Pergher, and D. A. G. Aranda, "Reaction kinetic study of solketal production from glycerol ketalization with acetone," *Industrial & Engineering Chemistry Research*, vol. 56, pp. 479–488, 2017.

[38] A. K. Singh and S. D. Fernando, "Reaction kinetics of soybean oil transesterification using heterogeneous metal oxide catalysts," *Chemical Engineering & Technology*, vol. 30, pp. 1716–1720, 2007.

[39] J. Zhang, J. Liu, X. Huang et al., "Heterogeneous catalytic esterification of oleic acid under sub/supercritical methanol over γ-Al2O3," *Fuel*, vol. 268, Article ID 117359, 2020.

[40] K. Sudsakorn, S. Saiwuttikul, S. Palitsakun, A. Seubsai, and J. Limtrakul, "Biodiesel production from Jatropha curcas oil using strontium-doped CaO/MgO catalyst," *Journal of Environmental Chemical Engineering*, vol. 5, pp. 2845–2852, 2017.

[41] Z. Derya, C. Velid, and D. Mesut, "Optimization and kinetic study of biodiesel production from jatropha curcas oil in supercritical methanol environment using ZnO/γ-Al_2O_3 catalyst," *Biomass Conversion and Biorefnery*, pp. 1–12, 2024.

[42] M. Jayakumar, K. B. Gebeyehu, K. V. Selvakumar, S. Parvathy, W. Kim, and N. Karmegam, "Waste Ox bone based heterogeneous catalyst synthesis, characterization, utilization and reaction kinetics of biodiesel generation from jatropha curcas oil," *Chemosphere*, vol. 288, Article ID 132534, 2022.

[43] A. S. Yusuff, L. T. Popoola, D. O. Adeniyi, and M. A. Olutoye, "Coal fly ash supported ZnO catalyzed transesterification of jatropha curcas oil: optimization by response surface methodology," *Energy Conversion and Management*, vol. 16, Article ID 100302, 2022.

[44] B. K. Highina, I. M. Bugaje, and B. Umar, "Biodiesel production from jatropha caucus oil in a batch reactor using zinc oxide as catalyst," *Journal of Petroleum Technology and Alternative Fuels*, vol. 2, no. 9, pp. 146–149, 2011.

[45] H. Pan, H. Li, X. F. Liu et al., "Mesoporous polymeric solid acid as efficient catalyst for (Trans)esterification of crude jatropha curcas oil," *Fuel Processing Technology*, vol. 150, pp. 50–57, 2016.

[46] S. H. Teo, U. Rashid, and Y. H. Taufiq-Yap, "Biodiesel production from crude jatropha curcas oil using calcium based mixed oxide catalysts," *Fuel*, vol. 136, pp. 244–252, 2014.

[47] F. Zhang, Z. Fang, and Y. T. Wang, "Biodiesel production direct from high acid value oil with a novel magnetic carbonaceous acid," *Applied Energy*, vol. 155, pp. 637–647, 2015.

[48] Y.-T. Wang, Z. Fang, X.-X. Yang et al., "One-step production of biodiesel from Jatropha oils with high acid value at low temperature by magnetic acid-base amphoteric nanoparticles," *Chemical Engineering Journal*, vol. 348, pp. 929–939, 2018.

[49] H. V. Lee, J. C. Juan, and Y. H. Taufiq-Yap, "Preparation and application of binary acid–base CaO–La_2O_3 catalyst for biodiesel production," *Renewable Energy*, vol. 74, pp. 124–132, 2015.

[50] Y. H. Taufiq-Yap, H. V. Lee, M. Z. Hussein, and R. Yunus, "Calcium-based mixed oxide catalysts for methanolysis of jatropha curcas oil to biodiesel," *Biomass Bioenergy*, vol. 35, pp. 827–834, 2011.

[51] Y. Liu, E. Lotero, J. G. Goodwin, and X. Mo, "Transesterification of poultry fat with methanol using Mg—Al hydrotalcite derived catalysts," *Applied Catalysis A: General*, vol. 331, pp. 138–148, 2007.

[52] B. Basumatary, S. Brahma, B. Nath, S. F. Basumatary, B. Das, and S. Basumatary, "Advances in CaO—based catalysts for sustainable biodiesel synthesis," *Green Energy and Resources*, vol. 1, no. 3, Article ID 101338, 2023.

[53] K. Saikia, K. Ngaosuwan, S. Assabumrungrat et al., "Sulphonated cellulose-based carbon as a green heterogeneous catalyst for biodiesel production: process optimization and kinetic studies," *Biomass and Bioenergy*, vol. 173, no. 2, Article ID 106799, 2023.

[54] S. Ao, B. Changmai, C. Vanlalveni, M. V. L. Chhandama, A. E. H. Wheatley, and S. L. Rokhum, "Biomass waste-derived catalysts for biodiesel production: recent advances and key challenges," *Renewable Energy*, vol. 223, Article ID 120031, 2024.